Surfaces and Interfaces 21 (2020) 100700

Contents lists available at ScienceDirect

Surfaces and Interfaces

journal homepage: www.elsevier.com/locate/surfin

Influence of copper doping on structural, morphological, optical, and vibrational properties of ZnO nanoparticles synthesized by sol gel method

Carolina Rojas-Michea[a,b], Mauricio Morel[c,*], Francisco Gracia[d], Gerardo Morell[e], Edgar Mosquera[f,g,*]

[a] Molecular Science Research Center, University of Puerto Rico, San Juan, Puerto Rico
[b] Department of Chemistry, University of Puerto Rico, San Juan, Puerto Rico
[c] Facultad de Ciencias Naturales and Instituto de Investigaciones Científicas y Tecnológicas, IDICTEC, Universidad de Atacama, Copiapó, Chile
[d] Departamento de Ingeniería Química, Biotecnología y Materiales, Facultad de Ciencias Físicas y Matemáticas, Universidad de Chile, Santiago, Chile
[e] Department of Physics and Institute for Functional Nanomaterials, University of Puerto Rico, San Juan, Puerto Rico
[f] Departamento de Física, Universidad del Valle, Cali, Colombia
[g] Centro de Excelencia en Nuevos Materiales (CENM) Universidad del Valle, Cali, Colombia

ARTICLE INFO

Keywords:
Cu-doped ZnO
Structural and optical properties
Vibrational spectroscopy
Photocatalytic studies

ABSTRACT

Cu-doped ZnO nanocrystals (with 0, 0.5, 1.0, 1.5, and 2.0 at.% Cu) have been successfully synthesized by a sol-gel method. The influence of Cu content on the properties of ZnO nanoparticles have been studied by various characterization techniques. XRD analysis reveals the formation of hexagonal wurtzite structure in all samples, confirming the incorporation of Cu ions into the ZnO lattice. The crystallite size and unit cell volume are modified with the Cu content. Morphology characterization by SEM and HRTEM revealed that Cu-doped samples consist of mixture of nanoparticles and nanowires. The energy band gap of the samples was red shift due to Cu incorporation in the ZnO lattice. The PL emission intensity of the Cu-doped samples decreases with increasing Cu content. Vibrational spectroscopy confirms metal oxide bond formation and reveals stress present in the samples. Under visible light illumination, the photocatalytic performance of all samples was studied by using methylene blue as a model molecule.

1. Introduction

In the last decades, nanostructured metal oxide semiconductors have been extensively studied due its unique and interesting characteristics observed only at nanoscale dimensions. Zinc oxide (ZnO) is an attractive semiconductor with a wide energy band gap (E_g ~ 3.37 eV) in the near ultraviolet and high-exciton binding energy (60 meV) which allows the excitonic transitions to occur even at room temperature (RT) [1–3]. In terms of new technological applications, several oxide materials, such as undoped and doped ZnO are being studied to establish correlation among structure, morphology and properties [4]. Therefore, ZnO has versatile applications in optoelectronics [5], sensing [6,7] and solar cells [8] to name some. Recently, doped ZnO nanostructures and other narrow energy band gap semiconductor nanomaterials have attracted significant attention for photocatalytic applications [9–16], where the effect of doping could greatly enhance the photocatalytic performance and absorb visible light to degrade various organic dyes in wastewater [1,2,14–17]. However, several methods such as sol-gel, hydrothermal, co-precipitation, mechanochemical process, microwave, and sonochemical, to name a few, are used to synthesize ZnO nanostructures [4,17–23]. Among them, the sol-gel method is commonly used ones due to their control over composition, structure, size and reproducibility. The properties of ZnO could be improved by adding doping elements such as Ag [24,25], Cu [15–17, 26–28], Al [29,30], In [31], Cr [32], and Mg [33]. In particular, the influence of Cu-doping on the optical properties of ZnO for enhancing the luminescence efficiency by creating localized impurity levels in the optical energy band gap has been reported previously [15,28,34]. Additionally, other studies affirm that the optical energy band gap is red shift when the average crystallite size is decreased due to the incorporation of Cu ions into the ZnO structure [28, 34–36].

Instead, it has been reported that the photocatalytic degradation activity of ZnO is improved by Cu addition up to 0.5% but decreased when increase the Cu addition to 1.0% [37]. Therefore, in this work the

* Corresponding author.
E-mail addresses: rojasmichea@gmail.com (C. Rojas-Michea), mauricio.morel.escobar@gmail.com (M. Morel), fgracia@ing.uchile.cl (F. Gracia), gmorell@gmail.com (G. Morell), edgar.mosquera@correounivalle.edu.co (E. Mosquera).

https://doi.org/10.1016/j.surfin.2020.100700
Received 16 March 2020; Received in revised form 4 September 2020; Accepted 10 September 2020
Available online 14 September 2020
2468-0230/ © 2020 Elsevier B.V. All rights reserved.

effect of low Cu^{2+} ion content (0.5, 1.0, 1.5 and 2.0%) inside the ZnO lattice has been studied. Different powerful techniques to evaluate the changes in the structural, optical, and photocatalytic properties of the samples were carried out. The samples were evaluated to study the photodegradation of Methylene blue (MB) organic dye under visible light illumination.

2. Experimental

2.1. Materials

The chemical materials used for synthesis of undoped and Cu-doped ZnO samples were of analytical grade without any further purification. High purity zinc nitrate ($Zn(NO_3)_2$•$6H_20$), copper nitrate ($Cu(NO_3)_2$•$3H_20$), and polyvinyl alcohol (PVA, Mw: 89,000 – 98,000 g mol^{-1}) were obtained from Sigma Aldrich, and absolute ethanol (purity of 99.5%) was obtained from Merck, Germany. The solvent used in the experiments was a mixture of deionized water and ethanol (ETOH, 50:50 vol).

2.2. Sample preparation

A sol-gel process reported in Ref [24] was used to prepare undoped and Cu-doped ZnO nanoparticles. Typically zinc nitrate, copper nitrate and PVA (8 g) were dissolved in a mixture of deionized water and ethanol (50:50) under magnetic stirring at 80 °C to prepare the corresponding gel solution. Finally, the samples were calcined at 600 °C for 8 h in air to achieve a homogeneous powder sample. In Table 1 are reported the molar ratios and molar composition for all samples and which have been obtained using XRF measurements.

2.3. Characterization techniques

The crystal structure of the prepared samples was characterized using a Bruker D8 X-ray diffractometer with $CuK\alpha_{1,2}$ (0.15428 nm) radiation at room temperature (RT) and operated at 40 kV and 30 mA. The morphological studies of the samples were investigated by using a scanning electron microscope (SEM, FEI Quanta 250) and transmission electron microscope (HRTEM, Tecnai F20 FEG-S/TEM) operate at 200 kV. X-ray Fluorescence were made through energy dispersive X-ray spectrometer Shimadzu (Rh X-ray, EDX-720) to determine the Zn and Cu percentage in the samples. Ultra-violet-visible (UV–vis) measurements of the prepared samples were recorded using a UV-2550 UV/Vis spectrometer Shimadzu in the range 300 – 800 nm. Surface area of the samples was determined by N_2 adsorption-desorption isotherms in an ASAP 2010 (Micromeritics, USA) system. Room temperature photoluminescence (RT-PL) measurements of the synthesized samples were performed in a Perkin Elmer spectrofluorometer LS-55, equipped with a Xenon lamp. A Rayleigh WQF-510A FTIR spectrophotometer was used to measure the IR spectra at room temperature and identify the functional groups in the samples. FTIR spectra were obtained using a solid solution with KBr. Raman spectra were recorded at room temperature in a Thermo scientific DXR smart Raman spectrometer with excitation wavelength of 532 nm (2.33 eV).

Table 1
Molar ratios and molar composition of Cu-doped ZnO nanoparticles.

Sample (at % Cu)	Weight (g) $Zn(NO_3)_2$	Weight (mg) Cu $(NO_3)_2$•$3H_2O$	Moles Zn:Cu	XRF Zn	Cu
0.5	4	0.0174	99.46:0.54	99.04(3)	0.54(3)
1.0	4	0.0336	98.97:1.03	98.55	1.05(1)
1.5	4	0.049	98.49:1.51	98.28(9)	1.33(7)
2.0	4	0.0658	97.97:2.03	97.64(2)	1.93(7)

2.4. Photocatalytic activity test

Photocatalytic activity on all samples was tested in a homemade reactor with 30 visible light (380–780 nm) lamps (50 W each) in 200 mL of aqueous methylene blue solution (MB, 5 ppm). In a typical experiment, 200 mg of photocatalyst was added to the MB aqueous solution under mixing by an air flow of 2.5 L min^{-1}. Adsorption/desorption equilibrium was achieved under dark conditions for 30 min before irradiation. A constant distance (23 cm) was maintained between the lamps (40.000 lux) and the solution, and the exposure time was varied under continuous agitation. After irradiation, small samples were centrifuged every 20 min and aliquots were collected to **measure the absorbance at 665 n**m (maximum absorption wavelength of MB). A correlation curve absorbance-MB concentration, based on the Beer-Lambert law was used to estimate the MB concentration during the photoactivity measurements.

3. Results and discussion

3.1. Structural and elemental study

Fig. 1 show the structural properties of undoped and Cu-doped ZnO nanoparticles grown by sol-gel method. The measurements were carried out through XRF and XRD **to determine** the elemental composition, crystalline phase and structure in the samples. By XRF measurements it was possible to determine the proportion of Cu on ZnO lattice (Table 1).

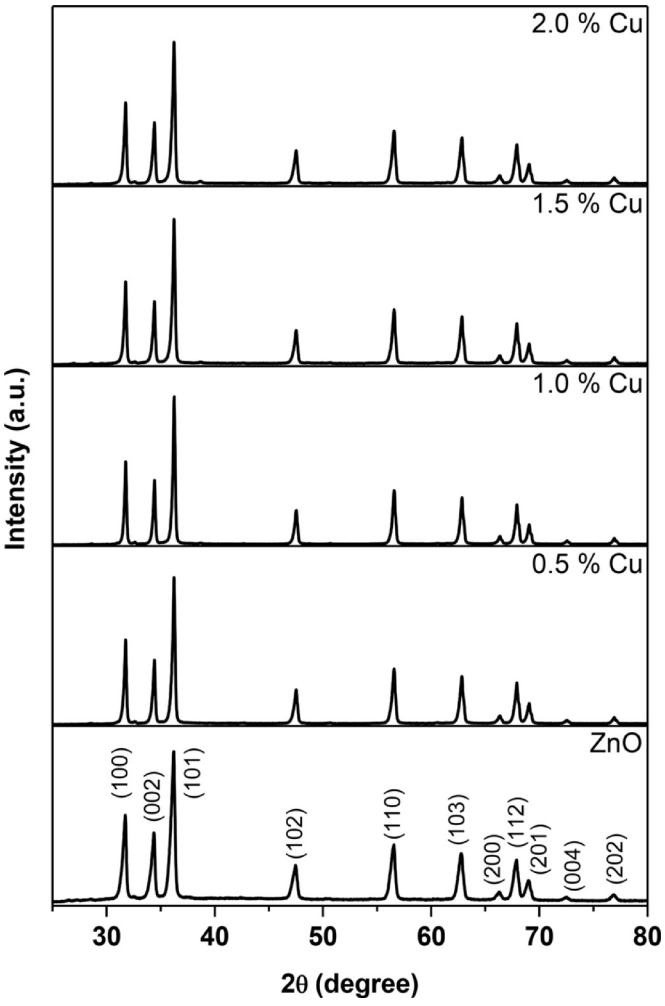

Fig. 1. X-ray diffraction patterns of ZnO and Cu-doped ZnO nanoparticles prepared by PVA-based sol gel synthesis.

Also, it was observed that the molar ratio and molar composition are in equal proportions confirming a good distribution of Cu atoms in the ZnO lattice. Instead, for ZnO nanoparticles the XRD patterns exhibited the characteristic peaks of a hexagonal wurtzite structure (JCPDS 79–0208 card [24]) and no other crystalline phases are detected, showing the purity of the sample. In Cu-doped ZnO, there are not presence of Cu phases (CuO, Cu_2O) or any binary zinc copper phase, indicating that Cu^{2+} ions (ionic radius of 0.73 Å) not change the crystalline structure of the ZnO. For all samples, the intense XRD peak located at around 2θ = 36.22°, 36.24°, 36.26°, 36.24°, and 36.24° corresponds to the preferential orientation of growth of the plane (101). As noted, all the samples have a polycrystalline structure. Also, the XRD patterns shows that preferred orientation is conserved with the increase of Cu-doping. However, all diffraction peaks are found to be sharp and intense which corresponding to a high crystallinity of the samples. Therefore, it was observed that in all samples there are solubility of Cu in ZnO. Our results agree with previous reports [28,38] where suggested that the solubility limit of Cu in ZnO is less than 5.0%.

The crystallite size (D_{hkl}) in all samples was determined from the line broadening (full-width at half-maximum, FWHM) of the (101) diffraction peak using the Scherrer´s formula (Eq. (1)) [39,40]:

$$D_{hkl} = \frac{k\lambda}{\beta_{hkl}\, cos\theta} \quad (1)$$

where, k (taken to be 0.9 for spherical particles [40]) is a shape factor, and λ (0.15405 nm) is the wavelength of the X-ray source, and β_{hkl} is the full width at half maximum (FWHM) of the diffraction peak. The average crystallite sizes of the samples have been found to be in 24 – 35 nm range, respectively. The position of the main diffraction peaks and average crystallite size are reported in Table 2. Fig. 2a shows the variation of both the average crystallite size and their FWHMs with the Cu content in all samples. With respect to ZnO lattice, it is observed that the crystallite size increase with Cu content and their FWHM decrease, indicating that there is an anisotropic growth of the grains induced by the Cu ions in the (101) preferable orientation. Fig. 2b shows the variation of the unit cell volume with the Cu content for the hexagonal wurtzite structure of ZnO. The values are summarized in Table 2. In addition, it is observed that for the Cu-doped samples there are a little variation of the volume in comparison with ZnO lattice. There is an increase of the volume for the sample with 0.5% of Cu content but, the values decrease for the samples with more Cu content (1.0, 1.5, 2.0 at% Cu), respectively. Lattice constants (a and c) and their ratio, c/a, for undoped and Cu-doped ZnO are calculated through Rietveld refinement and summarized in Table 2. Given that the parameters are consistent with a hexagonal wurtzite crystal structure and their change (structural deformation) is negligibly small in the samples, we suggest that the substitution of Cu into ZnO lattice is due to that their ionic radius (Cu^{2+}, 0.73 Å) is very close to that of Zn^{2+} (0.74 Å). In addition, copper doping reduces the lattice parameters and produces stress in the doped samples. No other phases were detected in the XRD pattern and the lattice parameters and volume of the unit cells match well with the JCPDS 79–0208 card [24].

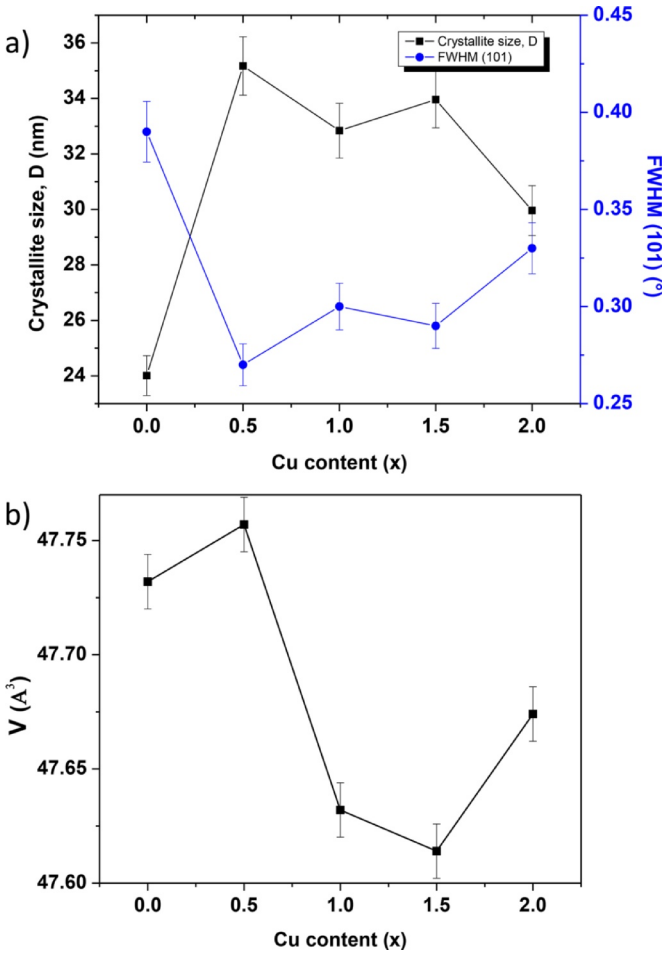

Fig. 2. (a) The crystalline size and FWHM of the plane (101) as function of Cu content. (b) The unit cell volume as function of the Cu content.

3.2. Morphological and surface studies

Morphological features of undoped and Cu-doped ZnO samples were investigated by scanning electron microscope (SEM) and transmission electron microscope (TEM), respectively. Fig. 3 shows the typical SEM micrographs of the synthesized Cu-doped ZnO nanocrystallites. As it can be seen, SEM images reveals that the samples are composed of particles with spherical morphology in predominant proportion and some 1D nanostructures, i.e., nanowires in less proportion. Our previous results suggested that spherical particles and 1D nanostructures could be synthesized via PVA-based sol-gel method [14]. In accordance with Ref [14], a higher or lower content of PVA is the cause of the morphology in the samples. However, it is the third time that our research group **reports a mixture of structures** by this method due to that there are similarities between the morphologies of the samples obtained. Moreover, high proportions ZnO/CuO nanocomposites have

Table 2
Position of the main diffraction peaks, average crystallite size and energy band gap values of all prepared samples.

Sample (at% Cu)	$ZnO_{(101)}$ peak position 2θ (°)	Crystallite size[a] D ± 1 (nm)	Lattice parameters a (Å)	c (Å)	c/a	Volume, V (Å^3)	Surface Area BET (m^2 g^{-1})	Absorption band edge (eV)
0	36.22	24	3.2524	5.2103	1.6019	47.732	3.5 ± 0.30	3.32
0.5	36.24	35	3.2531	5.2109	1.6018	47.757	3.8 ± 0.20	3.30
1.0	36.26	33	3.2507	5.2049	1.6012	47.632	8.0 ± 0.02	3.28
1.5	36.24	34	3.2486	5.2093	1.6036	47.614	7.8 ± 0.02	3.28
2.0	36.24	30	3.2512	5.2078	1.6018	47.674	7.3 ± 0.07	3.26

[a] Calculated by the Scherrer formula [39,40].

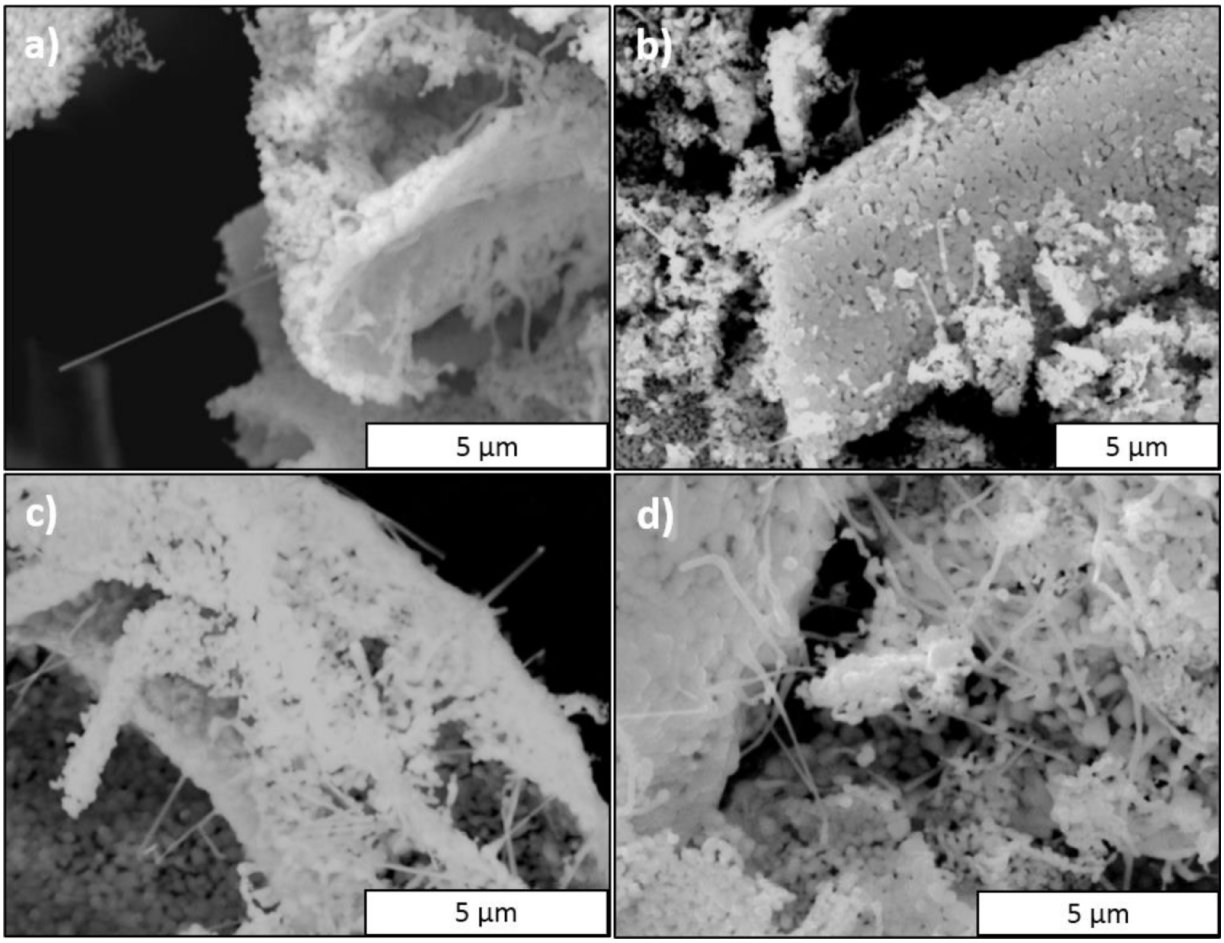

Fig. 3. SEM micrographs of Cu-doped ZnO with different Cu content. (a) 0.5, (b) 1.0, (c) 1.5, and (d) 2.0 at.% Cu.

been synthesized by our group via PVA-based sol-gel method and their properties studied [17]. In contrast with the results of the Ref [17], it was observed semi-spheroidal nanoparticles mixed with bigger rod-shape particles, confirming also that the morphology of the samples depends in part of the stability between PVA matrix and metallic ions.

TEM image of the sample with 0.5 at% Cu is shown in Fig. 4a-b. The white box in Figs. 4b shows the HRTEM images of the sample (Fig 4c-d). The results agree with XRD section, where the interplanar distance calculated from the images corresponds to 0.25 nm and match very well with the (101) crystalline plane of the hexagonal wurtzite structure of ZnO. Furthermore, there are formation of semi-spheroidal nanoparticles that could be the cause (act like seed) to grow long 1D nanostructures during the calcining process, see SEM images. Here, the heating rate could be an important factor to study.

Additionally, BET specific surface area were measured and compared between all samples. The values are reported in Table 2. The surface area (SA) of doped samples increases with Cu doping and is comparatively higher than ZnO sample. However, it is observed that for the sample at 1.0% of Cu content there are more formation of nanoparticles than 1D nanostructures, therefore, it could be increasing the SA. Instead, for the others Cu-doped samples there is a higher mix of nanostructures (particles and wires), then the SA decreased. Thus, the maximum SA value obtained was 8.0 $\pm$ 0.02 $m^2\ g^{-1}$ for sample with 1.0 at% Cu, respectively.

3.3. Optical properties

Room temperature UV-visible (UV–vis) absorption and photoluminescence (PL) studies were employed to know the optical properties of the samples. Fig. 5a displays the absorption spectra of the samples. It can be seen from Fig. 5a that for ZnO, the absorption peak appears at 374 nm (3.32 eV) and is attribute to the excitonic absorption determined from the equation $E_{exc} = hc/\lambda_{max}$ [11,14,24,28] where, h and c are the Planck´s constant and speed of light, respectively. While for Cu-doped samples the excitonic absorption peaks appear at 376 nm (3.30 eV), 378 nm (3.28 eV), and 380 nm (3.26 eV), for 0.5, 1.0, 1.5, and 2.0 at% Cu and indicating that the energy band gap (E_g) values decrease with increasing the Cu^{2+} ions content. Therefore, the E_g of the Cu-doped samples is slightly red shift with copper incorporation compared to that of ZnO, respectively. For pure ZnO, the E_g was 3.32 eV which matches with the value given in previous reports in literature. For Cu-doped samples, the E_g values found decrease by increasing the copper content (Table 2). The red shift, $\Delta E_g = (0.04 \pm 0.02)$ eV, in the energy band gap may be due to substitutional copper incorporated into the ZnO lattice [41,42].

In Fig. 6, the PL spectra for undoped and Cu-doped ZnO nanoparticles are shown. Here, all samples present a strong blue emission at 425 nm (2.92 eV) and ~ 488 nm (2.54 eV) accompanied by a weak green emission positioned at 529 nm (2.34 eV), respectively. The green emission is due to recombination of photo-generated hole and singly ionized oxygen [42,43]. Instead, the blue emission at 488 nm is due to the transition from Zn interstitials (Zni) to the valence band and the emission at 425 nm could be ascribed to singly ionized oxygen vacancy (V_o) [44,45]. On the other hand, a weak emission centered at 466 nm (2.65 eV) was observed in all samples, and its relative intensity decreases with increasing Cu content. A similar behavior was observed for emissions at 488, and 529 nm, respectively. Additionally, two weak violet emissions at around 370 (3.35 eV) and 406 nm (3.06 eV) was

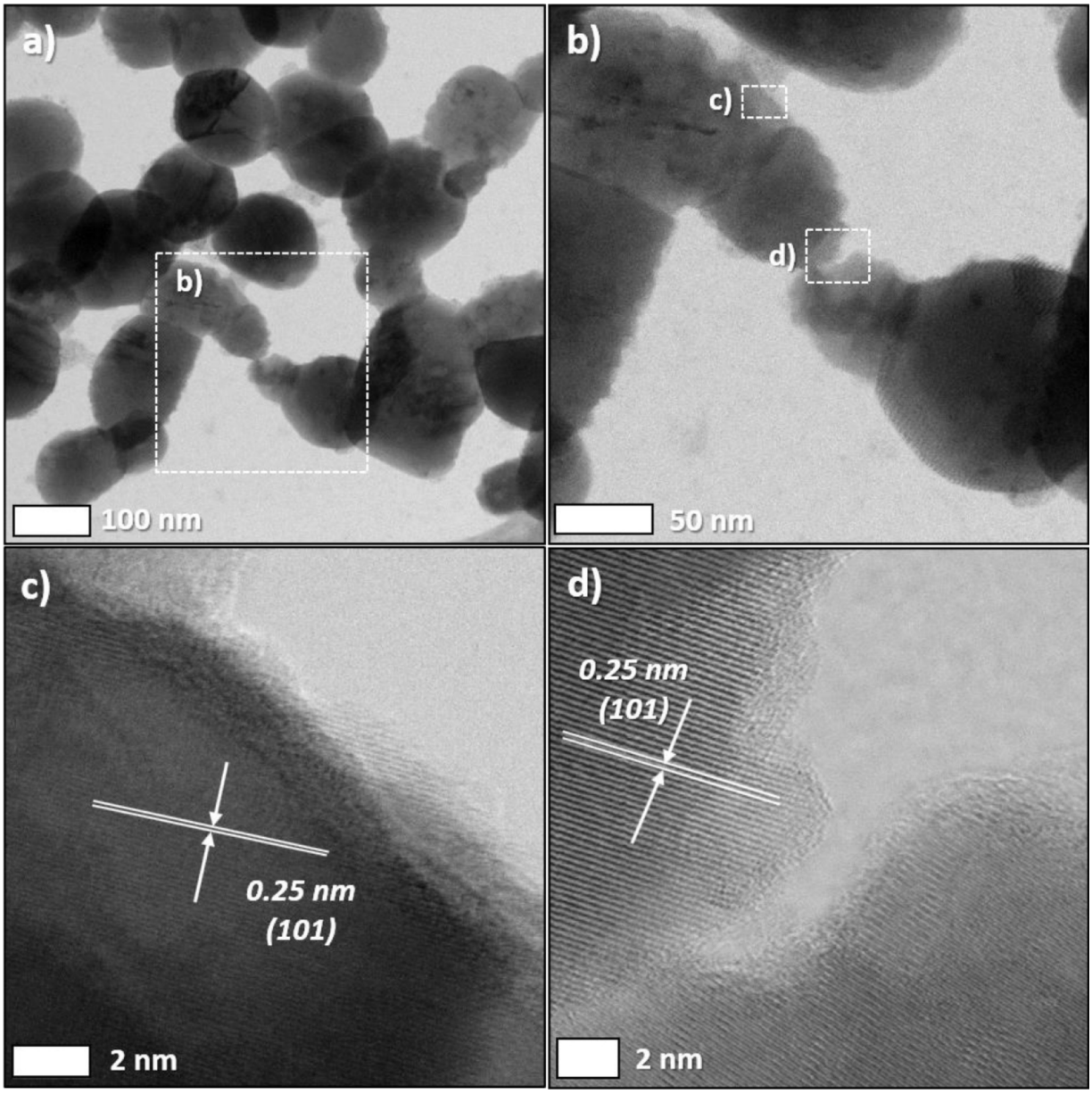

Fig. 4. TEM and HRTEM images of the sample with 0.5 at% Cu.

observed in the samples. The UV emission at ~ 370 nm could be associated with the variation of the E_g of ZnO nanoparticles. **Thus, the PL from the synthesized samples is strongly defect-dominated emission. In general, the energy transfer to certain impurities is quite slow, therefore, when the crystals contain many defects, the emission from doping ions will be weak. Instead, for defect-free crystals intense emission from doping ions can be obtained. In this case, if there are more oxygen vacancies (V_o) near to the surface of the samples, a weak emission from copper ions and weak energy transfer from the host to the copper ions can be expected. Furthermore, these oxygen vacancies (V_o) act as electron traps, preventing e^-/h^+ recombination, which could improve the photocatalytic behavior of ZnO samples.**

3.4. Vibrational spectroscopy

FTIR and Raman scattering spectra were investigated to elucidate the effect of Cu^{2+} doping on the vibrational properties of ZnO nanoparticles (Figs. 7 and 8). FTIR, characteristic bands of ZnO samples without doping and Cu-doped (from 1.0 to 2.0%) are listed in Table 3. **Fig. 7a shows the normalized transmittance and three specific zones (b-d). In Fig 7b and 7d, two vibrational modes are observed at around 1440 and 887 cm^{-1}, which can be assigned to carbonate species. Evans and Whateley [46] established the criteria to distinguish between the simple carbonate ion and the coordinated carbonate group. While, Du et al., [47] in a study reported the IR band positions for different carbonates species on various metal oxides, including hydrotalcite-like compounds. As well, they considered that the carbonate group may exist in salts or in complexes as a simple carbonate ion, or as a unidentate, bidentate, bridged, and polydentate surface carbonates [46,47]. In view of the above reports, the bands at 1440 and 887 cm^{-1} may be assign to non-coordinate (ν_3 vibrational mode) and to the ν_2 vibrational mode in the carbonate ion [46-48]. In addition, the single carbonate ion decreased drastically with the copper incorporation.** Instead, the bands around 600–400 cm^{-1} are attributed to metal–oxygen (M–O) stretching mode due to Zn–O and Cu–O vibrations [14,28,49]. In Fig. 7c, it is possible appreciate a decrease of the

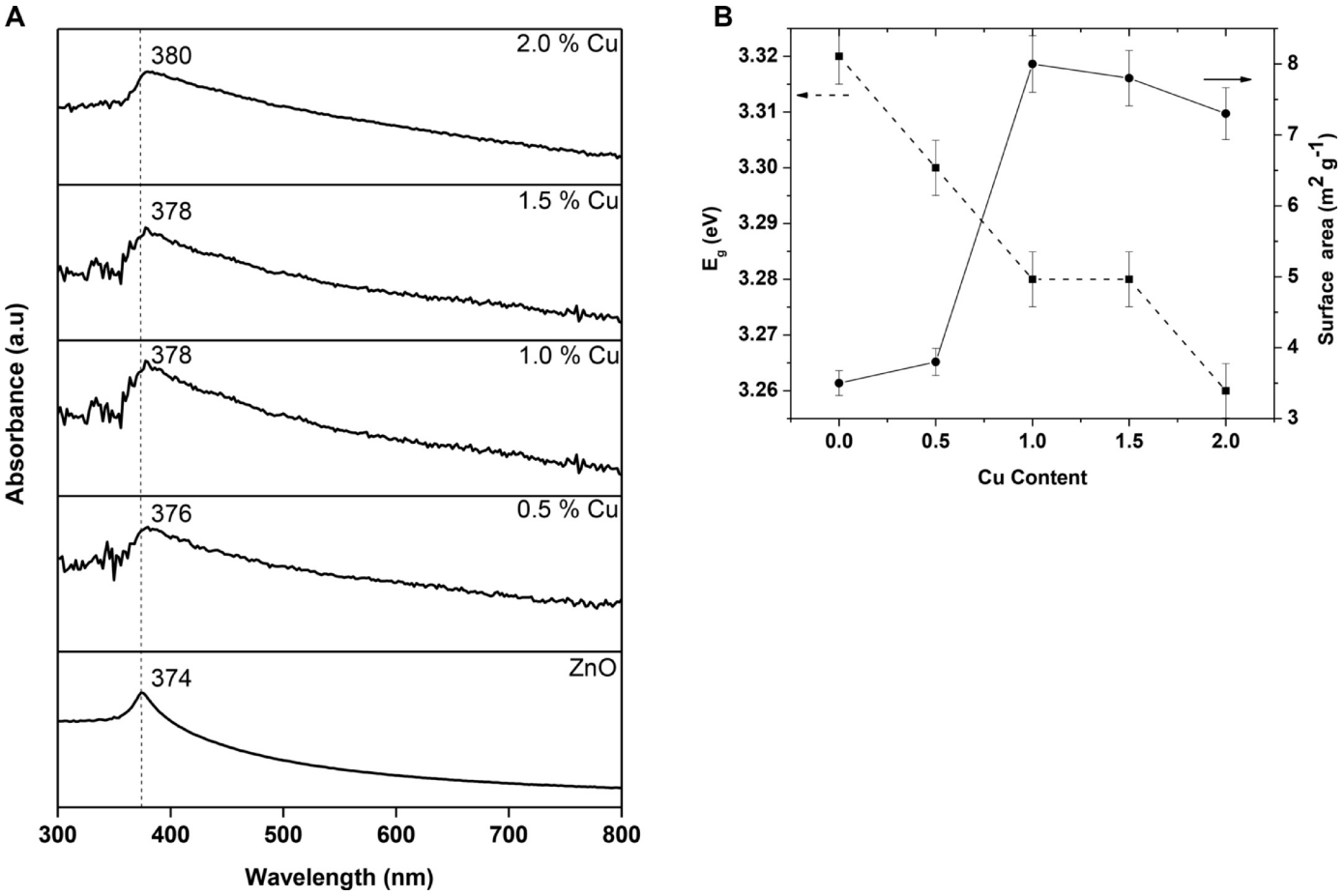

Fig. 5. (a) Room temperature UV–vis absorption spectra of all prepared samples. (b) The energy band gap and surface area as function of the Cu content.

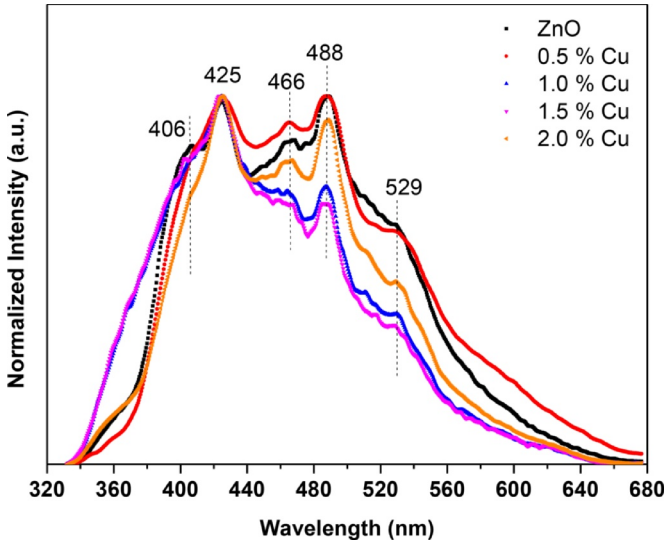

Fig. 6. Normalized photoluminescence spectra of all samples.

stretching mode of ZnO samples around 478 cm^{-1} due to the presence of the copper in all samples. Additionally, the sample with 1.5 at% Cu shows a signal at 1535 cm^{-1}, assigned to carboxylates from the PVA thermal decomposition [14].

Raman scattering has been employed to study the influence of Cu doping on ZnO structure. Fig. 8 shows the Raman spectra of the pure and Cu-doped ZnO nanoparticles and their assigned vibrational frequencies are listed in Table 4. As it is well known, in group theory the wurtzite-type ZnO (space group C_{6v}) has a sets of eight optical phonon modes at the Γ point of the Brillouin zone, represented as $A_1 + E_1 + 2E_2$ modes (Raman active), $2B_1$ modes (Raman silent) and $A_1 + E_1$ modes (infrared active), respectively. Both of A_1 and E_1 phonon modes are polar and they split into transverse-optical (TO) and longitudinal-optical (LO) phonons [1,24,28,50,51]. In according with the hexagonal wurtzite structure of ZnO, the $E_2^{(high)}$ optical phonon mode at 438 cm^{-1} (for the stress-free bulk ZnO) provides information on the stress in the sample. A decrease or increase in this mode is attributed to tensile or compressive stress in the crystal structure [3,28,51]. For ZnO nanoparticles, the $E_2^{(high)}$ mode was observed at 437 cm^{-1}, which is shifted by 1.0 cm^{-1} compared to bulk, and which is attributed to the tensile stress of the ZnO nanoparticles. While for Cu-doped ZnO, the samples also present a strong tensile stress due to incorporation of Cu^{2+} into ZnO lattice, see Table 4. However, the intensity $E_2^{(high)}$ phonon mode become broad and weaker, which means that the crystalline structure of ZnO is weakened (without significant deformation) with increasing copper doping. As can be seen, the observed FWHM due to dopant incorporation change indicating disorder into ZnO lattice [51].

For all doped samples, it is observed that the peak associated to E_2^{high}–E_2^{Low} phonon mode and which appears close to 330 cm^{-1} was vanished and red shifted while the A_1(TO) phonon mode disappear for a copper content bigger than 1.0%, respectively. In our case, the observed linewidth changes induced by Cu^{2+} are relatively bigger, indicating disorder introduced by copper ions into ZnO lattice. In addition, we observe that in ZnO spectrum the peaks at 330 cm^{-1} (E_2^{high}–E_2^{Low}) and 660 cm^{-1} (A_1) are second order Raman peaks corresponding to acoustic overtone, see Table 4. While the vibrational modes at 379 cm^{-1} and 540 cm^{-1} correspond to the symmetries A1 (TO) and A1 (LO), respectively.

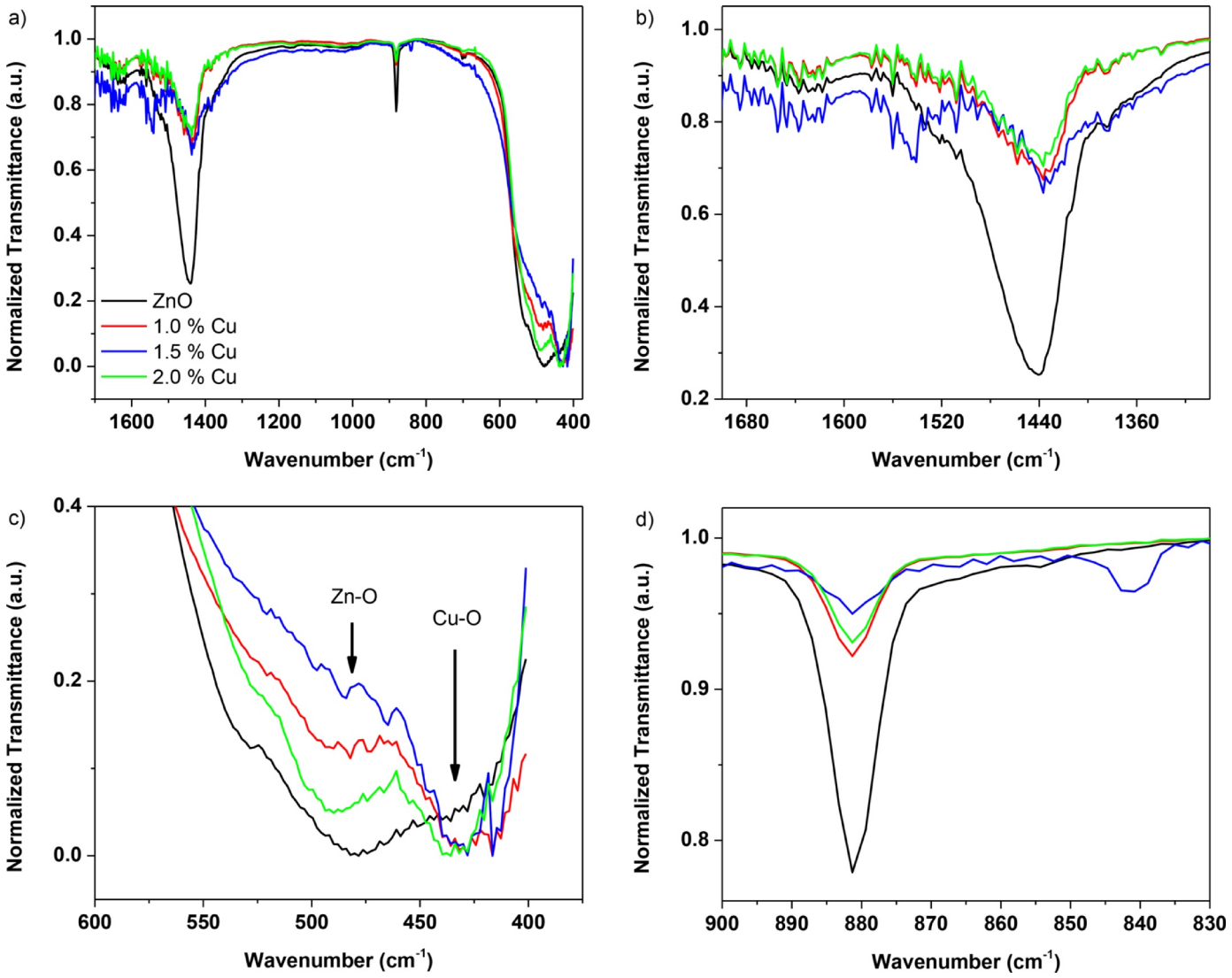

Fig. 7. (a)-(d) Infrared spectra of undoped and Cu-doped ZnO nanoparticles. (For interpretation of the references to colour in this figure legend, the reader is referred to the web version of this article.)

The observed peak at 587 cm^{-1} (E1(LO)) is associated with the impurities and structural defects (oxygen vacancies and Zinc interstitials) of the synthesized samples [3,28,51]. The broad features between 1079 cm^{-1} and 1155 cm^{-1} are assigned to the two-phonon modes characteristic of this II–IV semiconductor. The absence of copper oxides phases indicates that the Cu^{2+} ions substitute the Zn^{2+} sites doping the hexagonal wurtzite nanostructure of ZnO, which is consistent with the XRD results and other works [27,28,51,52].

3.5. Photocatalytic activity under visible light

The photocatalytic conversion of the samples with different Cu content was measured by photodegradation of methylene blue (MB) molecule under visible light irradiation during different times (0 – 220 min). Degradation by Cu-doped samples was compared with that of ZnO nanoparticles, see Fig. 9. Polat et al. [15] reports that Cu doping higher than 1.0 at.% increase the photocatalytic activity of ZnO under an UV light illumination. While Fu et al. [37] found that photocatalytic degradation increased for Cu-doped ZnO up to 0.5 at% and decreased for Cu-doped ZnO to 1.0 at%, respectively. The photocatalytic degradation mechanism of MB was also discussed in those studies. Instead, its observed that under visible light illumination, the photodegradation of MB remains around 90% for ZnO nanoparticles after 220 min in comparison with Cu-doped ZnO nanoparticles. This indicate that under visible irradiation the photocatalytic conversion percentage of MB in presence of ZnO nanoparticles is much faster than that Cu-doped ZnO nanoparticles. **Therefore, for the 1.0, 1.5 and 2.0% doped ZnO samples, the conversion percentages are less than 66% after 220 min, but for 0.5% doped samples, the value was 77%.** It is also noted that a higher Cu-doping concentration into ZnO reduces the photocatalytic activity. Therefore, for lower Cu content (less than 0.5 at % Cu) and under visible light illumination, doped samples show higher MB photodegradation activity, but still lower than that of pure ZnO due to a crystalline size effect.

4. Conclusions

In summary, a controlled amount of copper ions (0.5, 1.0, 1.5, and 2.0 at.% Cu) was successfully incorporated into ZnO nanoparticles by sol -gel method. XRD results confirms the substitution of copper ions in Zn sites without changing the wurtzite structure of ZnO**. Also, it was corroborated that the solubility limit of Cu in ZnO is at low concentration.** Morphological study reveals the formation of a mixtures of nanoparticles in predominant proportion and nanowires. TEM and RS results confirm the hexagonal wurtzite structure of ZnO and agree with XRD analysis. The energy band gap values decrease with increasing the

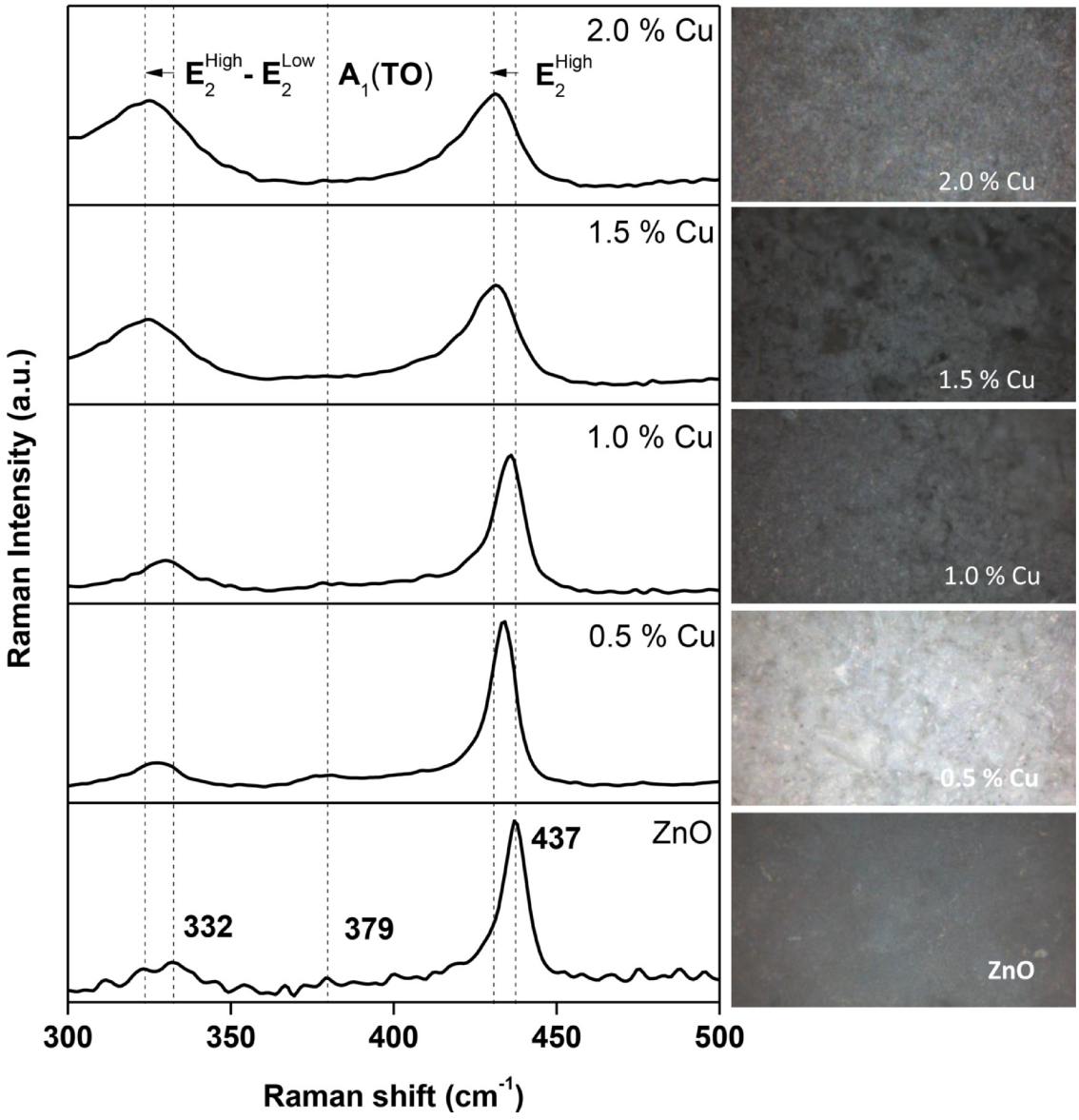

Fig. 8. Micro-Raman spectra of undoped and Cu-doped ZnO nanoparticles. Optical images from micro-Raman spectra (right).

Table 3
Infrared peaks and their assignments for ZnO and Cu-doped ZnO samples.

Assignments	Wavenumber (cm^{-1})				
	ZnO	0.5% Cu	1.0% Cu	1.5% Cu	2.0% Cu
O–H stretching	3438	3444	3457	3432	3430
O–H bending	1635	1635	1635	1637	1637
C = O stretching	1535	1531	1535	1544	1541
Carbonate ion CO_3 (ν_3 mode)	1440	1435	1440	1431	1437
Carbonate ion CO_3 (ν_2 mode)	881	879	881	–	881
Zn–O	478	478	482	487	487
Cu–O	–	–	426	428	426

Table 4
Experimental frequencies and symmetries of the modes found in Raman spectrum of wurtzite-type ZnO and Cu-doped ZnO nanoparticles and their assignments generating the peaks.

Raman Shift, ν_{exp} (cm^{-1})					Symmetry[c]
ZnO[b]	0.5% Cu	1.0% Cu	1.5% Cu	2.0% Cu	
190 (w)	202	205.6	202	198.8	2TA
332 (w)	328	329	325	325.1	$E_2^{High} - E_2^{Low}$
379 (vw)	382	379	–	–	A_1(TO)
437 (vs)	434	435	431	431	E_2(High)
540 (vw)	538	537.3	–	–	A_1(LO)
587 (vw)	582	575.8	574	571.9	E_1(LO)
660 (vw)	658	625	625	–	A_1
1079 (s)	1079	1078.2	–	–	A_1, E_2
1155 (w)	1150	1146.6	1130	1115.8	A_1

[b] Very weak (vw); weak (w), strong (s); very strong (vs).
[c] Ref [1,3,23,27,28,47,48,49,50].

Cu^{2+} ions content. Normalized PL showed that some relative emissions intensities decreases with increasing Cu content. **Raman spectra exhibit a shift to lower frequencies due to the copper content, confirming stress in samples. Under visible light illumination, the ZnO sample exhibits a better photocatalytic activity for MB degradation in comparison to doped samples. Doping reduces the energy gap of ZnO but does not achieve a better photodegradation of MB**

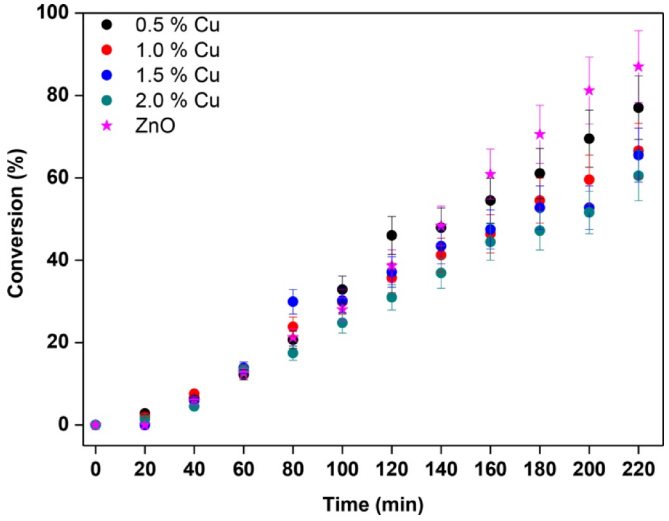

Fig. 9. Photocatalytic conversion percentage of MB under visible light illumination with all samples.

dyes. Here, the results are reproducible subject to strict control of the synthesis conditions.

Author statement form

Copyright Assignment The undersigned authors transfer all copyright ownership of this manuscript to the Journal Surfaces and Interfaces, in the event the work is published. The undersigned authors warrant the article is original, does not infringe upon any copyright or other proprietary right of any third party, is not under consideration for publication by any other journal, and has not been published previously. The authors confirm that they have reviewed and approved the final version of the manuscript.

Declaration of Competing Interest

The authors declare that they have no known competing financial interests or personal relationships that could have appeared to influence the work reported in this paper.

Acknowledgements

This work has been partially supported by the Chilean Government Research Agencies FONDECYT (No. 11110001 and No. 1150475), CONICYT-PIA (No. ACT1117), and FONDAP (No. 15110019 and No. 15090007), ANID-PAI77190056, and Universidad del Valle (C.I.71154). The authors thanks to Dr. F. Mendoza, Dr. K. Habiba, and Dr. R. Velázquez by characterization.

Supplementary materials

Supplementary material associated with this article can be found, in the online version, at doi:10.1016/j.surfin.2020.100700.

References

[1] X.B. Wang, C. Song, K.W. Geng, F. Zeng, F. Pan, Luminescence and Raman scattering properties of Ag-doped ZnO films, J. Phys. D: Appl. Phys. 39 (2006) 4992–4996 https://doi.org/10.1088/0022-3727/39/23/014.

[2] Ö.A. Yildirim, H.E. Unalan, C. Durucan, Highly efficient room temperature synthesis of silver-doped zinc oxide (ZnO:ag) nanoparticles: structural, optical, and photocatalytic properties, J. Am. Ceram. Soc. 96 (3) (2013) 766–773 https://doi.org/10.1111/jace.12218.

[3] E. Mosquera, J. Bernal, R.A. Zarate, F. Mendoza, R.S. Katiyar, G. Morell, Growth and electron field-emission of single-crystalline ZnO nanowires, Mater. Lett. 93 (2013) 326–329 https://doi.org/10.1016/j.matlet.2012.11.119.

[4] R. Bhardwaj, A. Bharti, J.P. Singh, K.H. Chae, N. Goyal, S. Gautam, Structural and electronic investigation of ZnO nanostructures synthesized under different environments, Heliyon 4 (2018) e00594 https://doi.org/10.1016/j.heliyon.2018.e00594.

[5] L. Schmidt-Mende, J.L. MacManus-Driscoll, ZnO – nanostructures, defects, and devices, Mater. Today 10 (2007) 40–48 https://doi.org/10.1016/S1369-7021(07)70078-0.

[6] M. Suchea, S. Christoulakis, K. Moschovis, N. Katsarakis, G. Kiriakidis, ZnO transparent thin films for gas sensor applications, Thin Solid Films 515 (2) (2006) 551–554 https://doi.org/10.1016/j.tsf.2005.12.295.

[7] A. Tamvakos, K. Korir, D. Tamvakos, D. Calestani, G. Cicero, D. Pullini, NO_2 gas sensing mechanism of ZnO thin-film transducers: physical experiment and theoretical correlation study, ACS Sens. 1 (4) (2016) 406–412 https://pubs.acs.org/doi/pdf/10.1021/acssensors.6b00051.

[8] N. Sekine, C.-.H. Chou, W.L. Kwan, Y. Yang, ZnO nano-ridge structure and its application in inverted polymer solar cell, Org. Electron. 10 (8) (2009) 1473–1477 https://doi.org/10.1016/j.orgel.2009.08.011.

[9] J. Saffari, N. Mir, D. Ghanbari, K. Khandan-Barani, A. Hassanabadi, M.R. Hosseini-Tabatabaei, Sonochemical synthesis of Fe_3O_4/ZnO magnetic nanocomposites and their application in photo-catalytic degradation of various organic dyes, J. Mater. Sci. Mater. Electron. 26 (12) (2015) 9591–9599 https://doi.org/10.1007/s10854-015-3622-y.

[10] G. Byzynski, C. Melo, D.P. Volanti, M.M. Ferrer, A.F. Gouveia, C. Ribeiro, J. Andrés, E. Longo, The interplay between morphology and photocatalytic activity in ZnO and N-doped ZnO crystals, Mater. Des. 120 (2017) 363–375 https://doi.org/10.1016/j.matdes.2017.02.020.

[11] R. Saravanan, N. Karthikeyan, V.K. Gupta, E. Thirumal, P. Thangadurai, V. Narayanan, A. Sthepen, ZnO/Ag nanocomposite: an efficient catalyst for degradation studies of textile effluents under visible light, Mater. Sci. Eng. C 33 (2013) 2235–2244 https://doi.org/10.1016/j.msec.2013.01.046.

[12] S.T. Kochuveedu, Y.H. Jang, D.H. Kim, A study on the mechanism for the interaction of light with noble metal-metal oxide semiconductor nanostructures for various photophysical applications, Chem. Soc. Rev. 42 (2013) 8467–8493 https://doi.org/10.1039/c3cs60043b.

[13] A. Di Paola, E. García-López, G. Marcí, L. Palmisano, A survey of photocatalytic materials for environmental remediation, J. Hazard. Mater. 211-212 (2012) 3–29 https://doi.org/10.1016/j.jhazmat.2011.11.050.

[14] E. Mosquera, I. del Pozo, M. Morel, Structure and red shift of optical band gap in CdO-ZnO nanocomposite synthesized by the sol gel method, J. Solid State Chem. 206 (2013) 265–271 https://doi.org/10.1016/j.jssc.2013.08.025.

[15] I. Polat, S. Yilmaz, I. Altin, E. Bacaksiz, M. Sokmen, The influence of Cu-doping on structural, optical and photocatalytic properties of ZnO nanorods, Mater. Chem. Phys. 148 (2014) 528–532 https://doi.org/10.1016/j.matchemphys.2014.07.011.

[16] J.-.H. Huang, J.-.X. Chen, Y.-.F. Tu, Y. Tian, D. Zhou, G. Zheng, J.-.P. sang, Q.-.M. Fu, Preparation and photocatalytic activity of CuO/ZnO composite nanostructured films, Mater. Res. Express 6 (2018) 1 https://doi.org/10.1088/2053-1591/aae6ff.

[17] A. Lavín, R. Sivasamy, E. Mosquera, M.J. Morel, High proportion ZnO/CuO nanocomposites: synthesis, structural and optical properties, and their photocatalytic behavior, Surfaces Interfaces 17 (2019) 100367https://doi.org/10.1016/j.surfin.2019.100367.

[18] R. Kripal, A.K. Gupta, R.K. Srivastava, S.K. Mishra, Photoconductivity and photoluminescence of ZnO nanoparticles synthesized via co-precipitation method, Spectrochim. Acta Part A: Mol. Biomol. Spectrosc. 79 (5) (2011) 1605–1612 https://doi.org/10.1016/j.saa.2011.05.019.

[19] A. Tadjarodi, M. Izadi, M. Imani, Synthesis and characterization of the special ZnO nanostructure by mechanochemical process, Mater. Lett. 92 (2013) 108–110 https://doi.org/10.1016/j.matlet.2012.10.045.

[20] L.Y. Yang, S.Y. Dong, J.H. Sun, J.L. Feng, Q.H. Wu, S.P. Sun, Microwave-assisted preparation, characterization and photocatalytic properties of a dumbbell–shaped ZnO photocatalyst, J. Hazard. Mater. 179 (1–3) (2010) 438–443 https://doi.org/10.1016/j.jhazmat.2010.03.023.

[21] M.M. Ba-abbad, A. Amir, H. Kadhum, A. Bakar, M.S. Takriff, The effect of process parameters on the size of ZnO nanoparticles synthesized via the sol–gel technique, J. Alloy. Compd. 550 (2013) 63–70 https://doi.org/10.1016/j.jallcom.2012.09.076.

[22] A.E. Kandjani, M.F. Tabriz, B. Pourabbas, Sonochemical synthesis of ZnO nanoparticles: the effect of temperature and sonication power, Mater. Res. Bull. 43 (3) (2008) 645–654 https://doi.org/10.1016/j.materresbull.2007.04.005.

[23] D. Polsongkram, P. Chamninok, S. Pukird, L. Chow, O. Lupan, G. Chai, H. Khallaf, S. Park, A. Schulte, Effect of synthesis conditions on the growth of ZnO nanorods via hydrothermal method, Phys. B: Condens. Matter 403 (19–20) (2008) 3713–3717 https://doi.org/10.1016/j.physb.2008.06.020.

[24] E. Mosquera, C. Rojas-Michea, M. Morel, F. Gracias, V. Fuenzalida, R. Zárate, Zin oxide nanoparticles with incorporated silver: structural, morphological, optical and vibrational properties, Appl. Surf. Sci. 347 (2015) 561–568 https://doi.org/10.1016/j.apsusc.2015.04.148.

[25] S. Khosravi-Gandomani, R. Yousefi, F. Jamali-Sheini, N.M. Huang, Optical and electrical properties of p-type Ag-doped ZnO nanostructures, Ceram. Int. 40 (6) (2014) 7957–7963 https://doi.org/10.1016/j.ceramint.2013.12.145.

[26] Y.M. Tao, S.Y. Ma, H.X. Chen, J.X. Meng, L.L. Hou, Y.F. Jia, X.R. Shang, Effect of the oxygen pressure on the microstructure and optical properties of ZnO:cu films, Vacuum 85 (2011) 744–748 https://doi.org/10.1016/j.vacuum.2010.11.009.

[27] J. Iqbal, N. Safdar, T. Jan, M. Ismail, S.S. Hussain, A. Mahmood, S. Shahzad, Q. Mansoor, Facile synthesis as well as structural, Raman, dielectric and

antibacterial characteristics of Cu doped ZnO nanoparticles, J. Mater. Sci. Technol. 31 (3) (2015) 300–304 https://doi.org/10.1016/j.jmst.2014.06.013.
[28] A.A. Othman, M.A. Ali, E.M.M. Ibrahim, M.A. Osman, Influence of Cu doping on structural, morphological, photoluminescence, and electrical properties of ZnO nanostructures by ice-bath assisted sonochemical method, J. Alloy. Compd. 683 (2016) 399–411 https://doi.org/10.1016/j.jallcom.2016.05.131.
[29] A. Anopchenko, S. Gurung, L. Tao, C. Arndt, H.W.H. Lee, Atomic layer deposition of ultra-thin and smooth Al-doped ZnO for zero-index photonics, Mater. Res. Express 5 (2018) 014012https://doi.org/10.1088/2053-1591/aaa653.
[30] J. Ghosh, R. Ghosh, P.K. Giri, Chemical tuning the visible photoluminescence in Al doped ZnO thin films and its application in label-free glucose detection, Sens. Actuators B Chem. 254 (2018) 681–689 https://doi.org/10.1016/j.snb.2017.07.110.
[31] K. Mohmood, A. Khalid, S.W. Ahmad, M.T. Mehran, Indium-doped ZnO mesoporous nanofibers as efficient electron transporting materials for perovskite solar cells, Surface Coating Technol. 352 (2018) 231–237 https://doi.org/10.1016/j.surfcoat.2018.08.039.
[32] E. Manikandan, V. Murugan, G. Kavitha, P. Babu, M. Maaza, Nano flower rod wire-like structures of dual metal (Al and Cr) doped ZnO thin films: structural, optical and electronic properties, Mater. Lett. 131 (2014) 225–228 https://doi.org/10.1016/j.matlet.2014.06.008.
[33] K. Pradeev raj, K. Sadaiyandi, A. Kennedy, S. Sagadevan, Z.Z. Chowdhury, M.R.B. Johan, F.A. Aziz, R.F. Rafique, R.T. Selvi, R.R. Bala, Influence of Mg doping on ZnO nanoparticles for enhanced photocatalytic evaluation and antibacterial analysis, Nanoscale Res. Lett. 13 (2018) 229 https://doi.org/10.1186/s11671-018-2643-x.
[34] S. Muthukumaran, R. Gopalakrishnan, Structural. FTIR and photoluminescence studies of Cu doped ZnO nanopowders by co-precipitation method, Opt. Mater. 34 (2012) 1946–1953 https://doi.org/10.1016/j.optmat.2012.06.004.
[35] A.J. Reddy, M.K. Kokila, H. Nagabhushana, R.P.S. Chakradhar, C. Shivakumara, J.L. Rao, B.M. Nagabhushana, Structural, optical and EPR studies on ZnO: cu nanopowders prepared via low temperature solution combustion synthesis, J. Alloy. Compd. 509 (17) (2011) 5349–5355 https://doi.org/10.1016/j.jallcom.2011.02.043.
[36] M. Mittal, M. Sharma, O.P. Pandey, UV-Visible light induced photocatalytic studies of Cu doped ZnO nanoparticles prepared by co-precipitation method, Sol. Energy 110 (2014) 386–397 https://doi.org/10.1016/j.solener.2014.09.026.
[37] M. Fu, Y. Li, S. Wu, P. Lu, J. Liu, F. Dong, Sol-gel preparation and enhanced photocatalytic performance of Cu-doped ZnO nanoparticles, Appl. Surf. Sci. 258 (2011) 1587–1591 https://doi.org/10.1016/j.apsusc.2011.10.003.
[38] H. Lee, B. Kim, C.R. Cho, S. Jeong, A study of magnetic and optical properties of Cu-doped ZnO, Phys. Stat. Sol. B 241 (2004) 1533–1536 https://doi.org/10.1002/pssb.200304614.
[39] B.D. Cullity, Elements of X-Ray Diffraction, 2nd Ed., Addison Wesley, 1978.
[40] A.L. Patterson, The Scherrer formula for X-ray particle size determination, Phys. Rev. 56 (1939) 978–982 https://doi.org/10.1103/PhysRev.56.978.
[41] M. Sajjad, I. Ullah, M.I. Khan, J. Khan, M.Y. Khan, M.T. Qureshi, Structural and optical properties of pure and copper doped zinc oxide nanoparticles, Results in Physics 9 (2018) 1301–1309 https://doi.org/10.1016/j.rinp.2018.04.010.
[42] P.K. Samanta, A.K. Bandyopaghyay, Chemcal growth of hexagonal zinc oxide nanorods and their optical properties, Appl. Nanosci. 2 (2012) 111–117 https://link.springer.com/article/10.1007/s13204-011-0038-8.
[43] B. Lin, Z. Fu, Y. Jia, Green luminescent center in undoped zinc oxide films deposited on silicon substrates, Appl. Phys. Lett. 79 (2001) 943–945 https://doi.org/10.1063/1.1394173.
[44] P.S. Xu, Y.M. Sun, C.S. Shi, F.Q. Xu, H.B. Pan, The electronic structure and spectral properties of ZnO and its defects, Nucl. Instrum. Methods Phys. Res. B. 199 (2003) 286–290 https://doi.org/10.1016/S0168-583X(02)01425-8.
[45] Z. Fang, Y. Wang, D. Xu, Y. Tan, X. Liu, Blue luminescent center in ZnO films deposited on silicon substrates, Opt. Mater. 26 (2004) 239–242 https://doi.org/10.1016/j.optmat.2003.11.027.
[46] J.V. Evans, T.L. Whateley, Infra-red study of adsorption of carbon dioxide and water on magnesium oxide, Trans. Faraday Soc. 63 (1967) 2769–2777 https://doi.org/10.1039/TF9676302769.
[47] H. Du, C.T. Williams, A.D. Ebner, J.A. Ritter, In situ FTIR spectroscopy analysis of carbonate transformations during adsorption and desorption of CO2 in K-promoted HTlc, Chem. Mater. 22 (2010) 3519–3526, https://doi.org/10.1021/cm100703e.
[48] W.N.R.W. Isahak, Z.A.C. Ramli, M.W. Ismail, K. Ismail, R.M. Yusop, M.W.M. Hisham, M.A. Yarmo, Adsorption–desorption of CO_2 on different type of copper oxides surfaces: physical and chemical attractions studies, J. CO2 Utilization. 2 (2013) 8–15 https://doi.org/10.1016/j.jcou.2013.06.002.
[49] R. Saravanan, S. Karthikeyan, V.K. Gupta, G. sekaram, V. Narayanan, A. Stephen, Enhanced photocatalytic activity of ZnO/CuO nanocomposite for the degradation of textile dye on visible light illumination, Mater. Sci. Eng. C 33 (2013) 91–98 https://doi.org/10.1016/j.msec.2012.08.011.
[50] L.N. Wang, L.Z. Hu, H.Q. Zhang, Y. Qiu, Y. Lang, G.Q. Liu, J.Y. Ji, J.X. Ma, Z.W. Zhao, Studying the Raman spectra of Ag doped films grown by PLD, Mater. Sci. Semicond. Proc. 14 (2011) 274–277 https://doi.org/10.1016/j.mssp.2011.05.004.
[51] O. Marín, T. Soliz, J.A. Gutiérrez, M. Tirado, C. Figueroa, D. Comedi, Structural, optical and vibrational properties of ZnO:m (M = Al^{3+} and Sr^{2+}) nano and micropowders grown by hydrothermal synthesis, J. Alloys Compd. 789 (2019) 56–65 https://doi.org/10.1016/j.jallcom.2019.03.115.
[52] L. Chow, O. Lupan, G. Chai, H. Khallaf, L.K. Ono, B. Roldan Cuenya, I.M. Tiginyanu, V.V. Ursaki, V. Sontea, A. Schulte, Synthesis and characterization of Cu-doped ZnO one-dimensional structures for miniaturized sensor applications with faster response, Sens. Actuators, A Phys. 189 (2013) 399–408 https://doi.org/10.1016/j.sna.2012.09.006.